Meteorological measurements and fire weather conditions—RxCADRE

Craig B. Clements[A,E], *Neil Lareau*[A], *Daisuke Seto*[A], *Jon Contezac*[A], *Braniff Davis*[A], *Casey Teske*[B], *Bret Butler*[C], *Dan Jimenez*[C], *and J. Kevin Hiers*[D]

[A]San José State University, Department of Meteorology and Climate Science, Fire Weather Research Laboratory, San José, CA USA

[B]College of Forestry and Conservation, The University of Montana, National Center for Landscape Fire Analysis, Missoula, MT USA

[C]USDA Forest Service, Fire Sciences Laboratory, Missoula, MT USA

[D]Wildland Fire Center, US Air Force, Eglin AFB, Niceville, FL, USA

[E]Corresponding author. Email: craig.clements@sjsu.edu

Abstract

To evaluate and test the next generation of wildland fire models, the Prescribed Fire Combustion and Atmospheric Dynamics Research Experiment (RxCADRE) focused on measuring fire-atmosphere interactions. The RxCADRE campaign conducted a series of prescribed fires over the course of two weeks in November 2012 at Eglin Air Force Base in north Florida, with an objective of capturing simultaneous effects of fine- to coarse-scale fuels and analyzing fire-atmosphere interactions. Preliminary results show that the meteorological measurement campaign captured both the fire weather conditions that influenced the experiments and the local fire-atmosphere interactions at the fire front. Usage of a Doppler lidar shows fire-induced circulations occurred during the L2G burn, where strip head fires created a merged plume. A region of decreased radial velocities and reversed flow was observed to occur downwind of the plume and was most likely associated with the development of a convergence zone forming in response to instabilities associated with the fire front. Overall, the RxCADRE campaign gives researchers another dataset with which to study atmospheric turbulent structures/fluxes associated with different fuel types, and provides a basis to further our understanding of the dynamics of fire-atmosphere interactions.

Summary

Meteorological observations were made during the RxCADRE campaign using both in situ and remote sensing sensor arrays. The measurements provide comprehensive high-spatial resolution data sets for coupled fire-weather model initialization and evaluation. Preliminary results indicate that the low-intensity fires conducted during the campaign were associated with weak fire-atmosphere interactions.

Keywords: Fire-atmosphere interactions, fire weather, Doppler lidar, micrometeorology

Introduction

One of the core objectives of the Prescribed Fire Combustion and Atmospheric Dynamics Research Experiment (RxCADRE) field campaign focused exclusively on coupled fire-atmospheric measurements to test and evaluate the next generation of fire models. To achieve this goal during the 2012 field campaign, many instrument platforms were deployed to measure both the ambient fire weather conditions and the fire-atmosphere interactions associated with the fires and plumes. Fire-atmosphere interactions are defined as the interactions between presently burning fuels and the atmosphere, in addition to interactions between fuels that will eventually burn in a given fire and the atmosphere (Potter 2012).

Currently, much of the meteorological sampling for fire behavior applications and science is performed at a very coarse resolution (i.e., hundreds of meters to kilometers), such as standard remote automated weather station networks in existence throughout the United States (Horel and Dong 2010). However, there is an increasing need to measure fire-atmosphere interactions at finer scales to better understand the role of near-surface wind and thermodynamic structures of fire behavior (Clements *et al.* 2007) and provide evaluation datasets for new-generation coupled fire-atmosphere modeling systems (Kochanski *et al.* 2013; Filippi *et al.* 2013; Coen *et al.* 2013).

To date, few field experiments have focused on the simultaneous measurement of fire behavior and fine-scale meteorology. The FireFlux experiment (Clements *et al.* 2007, 2008; Clements 2010), provided the first dataset of in situ micrometeorological measurements during a fire front passage (FFP). While the FireFlux dataset remains the standard for the evaluation of coupled fire-weather models (e.g., Kochanski *et al.* 2013; Filippi *et al.* 2013), it is limited by a lack of comprehensive fire behavior measurements. Therefore, more comprehensive field experiments are required to better understand the role of fire-atmosphere interactions on fire spread. To that end, an extensive set of meteorological instruments was deployed simultaneously with a comprehensive suite of fire behavior measurements that included multiple airborne and in situ ground based platforms. The RxCADRE campaign provided a series of prescribed fires conducted over the course of two weeks in various fuels with an objective of capturing simultaneous effects of fine- to coarse-scale fuels and atmospheric influences.

The goal of this paper is to describe the overall meteorological measurement campaign design and methods and present initial results from analyses of two burn experiments. The paper is organized as follows: experimental design and instrumentation used, results from one of the smaller burn units (S5) and one of the larger burn units (L2G), and conclusions and summary.

Experimental design and instruments

The RxCADRE meteorological measurement campaign consisted of a variety of measurement platforms and instrument types. The experimental design was aimed at measuring both the ambient meteorological conditions surrounding each burn plot and the in situ fire-atmosphere interactions within the burn plots. Table 1 lists each instrument used for meteorological measurements. The wind field was measured extensively using several instruments and platforms, including a scanning Doppler wind lidar, an array of cup-and-vane anemometers around each burn unit perimeter, an interior tower equipped with two sonic anemometers (Fig 1*a*), a Doppler mini-Sodar wind profiler, and a portable, 30-m meteorological tower (Fig. 1*b*) placed outside of all the burn units (except during the L1G burn on 3 November 2012, where the tower was placed in the middle of the burn unit). Table 2 lists cup-and-vane anemometer spacing and ignition information for each burn unit.

The CSU-MAPS

The California State University-Mobile Atmospheric Profiling System (CSU-MAPS) was deployed during the entire field campaign (Fig. 1*c*). The CSU-MAPS consists of several platforms and sensor types including a scanning Doppler lidar, microwave temperature and humidity profiler, and surface weather station, all mounted on a Ford F-250 4x4 truck. In addition to the remote sensing platforms, a portable 30-m meteorological tower mounted on a dual-axle trailer (Fig. 1*b*) was equipped at four levels with thermistor-hygristor probes to measure temperature and humidity (Vaisala, Inc., HMP-45C) and 2-d sonic anemometers (Gill Windsonic). Additionally, two 3-d sonic anemometers (R.M. Young, 81000) were mounted on the tower at 7 m and 31 m AGL. A more detailed overview of the CSU-MAPS is provided in Clements and Oliphant (2014).

The key instrument of the CSU-MAPS is a pulsed Doppler lidar (Halo Photonics, Ltd., model Streamline 75). The lidar emits an eye-safe infrared light at a wavelength of 1.5 μm (Pearson *et al.* 2009, 2010). The system is equipped with an all-sky optical scanner, enabling the lidar to scan from 0 to 360° in azimuth angle and -15 to 195° in elevation angle. The range gate is 18 m with a minimum range of 80 m and a potential maximum range of 9.6 km, typically associated with heavy aerosol targets such as clouds. The lidar provides radial velocities along the path of the beam. The CSU-MAPS is also equipped with a microwave temperature and humidity profiler that provides a continuous sounding from the surface to 10 km AGL by observing atmospheric brightness temperatures in 21 K-band channels and 14 V-band channels (Ware *et al.* 2003). Data from the microwave profiler are not discussed in this paper. Upper-air soundings were made using radiosondes (Vaisala, Inc, RS-92GPS) that were launched on site just before and after each burn period.

Doppler mini SoDAR

An Atmospheric Research & Technology, LLC, model VT-1 Doppler mini SoDAR was used to characterize the surface layer wind profiles up to 200 m AGL. The VT-1 was placed upwind of each burn block to measure the ambient profile of wind entering the experimental site. The SoDAR was configured to provide 10 min average profiles of wind speed and direction from 15 to 200 m AGL.

Surface anemometer array

A network of surface cup-and-vane anemometers were set up with approximately 20-m spacing around each small burn block, with adjacent burn block edges sharing anemometers. These instruments were mounted at 3.3 m AGL. The data are used to characterize surface flow patterns before and during the burns. Cup revolutions and unit vector components were sampled at a frequency of 3 s. Wind speed is the average speed for the entire logging interval. Gust speed is the highest three-second wind recorded during the logging interval. Average direction is calculated from the average of the vector components. The three large burn blocks were also instrumented with cup-and-vane anemometers at 150- or 300-m spacing around the perimeters. Three highly- instrumented plots (HIPs) were placed within each of the large burn blocks, and each of the HIPs had an anemometer located nearby (within the burn unit) in plots L2F and L2G. In addition to the standard spacing, all of the large burn blocks had additional anemometers placed to capture variability. Block L1G had a concentration of anemometers spaced about 50 to 75 m apart around the east corner to attempt to capture surface layer flow variability due to canopy effects (Fig. 2). Additionally, anemometers were placed roughly perpendicular to the interior firebreak road between L2F and L2G, with three on each side of the road, to assess the effects of the canopy on surface flow.

Micrometeorological tower

To capture the near-surface micrometeorology of the passing fire front, a guyed steel tower instrumented with anemometers, thermocouples, and heat flux sensors was deployed inside each of the nine burn units; the tower was 9.1 m for the forested burn unit (L2F) and 6.1 m for all other burn units. Two 3-d sonic anemometers (Applied Technology Inc., SATI Sx probe), were mounted at the height of 5.8 m and 2.0 m AGL (8.7 m and 3.8 m AGL for L2F). An array of fine-wire thermocouples (Omega, Inc. 5SC, Type-E) was used to measure plume and near-surface temperature profiles. The thermocouples were placed every meter from 1 m AGL to the top of the towers. Total and radiative heat fluxes were measured using a Schmidt-Boelter gauge total heat flux sensor (Hukseflux, SBG01) and a Gardon gauge radiant heat flux sensor (Medtherm, 64P-50-24), respectively. All tower data were recorded using a Campbell Scientific, Inc. CR3000 datalogger mounted near the base of the tower housed in an environmental enclosure, and the tower bases were protected from the extreme heat of the fire using fire shelter material. The fire front was allowed to burn directly underneath the towers.

Observations and results

In this section we describe the synoptic environment and boundary-layer evolution of each burn day. In addition, preliminary results from the S5 and L2G burn blocks, illustrating key measurement platform performance and observed fire-atmosphere interactions are discussed.

Synoptic environment and boundary-layer structure

The controlled burns were conducted from mid-morning (about 1600 UTC) through early afternoon (about 2200 UTC) on 1, 4, 7, 10, and 11 November 2012. The large-scale patterns of wind, temperature, and pressure affecting northern Florida during each burn are summarized in this section. We also examine pre- and post-burn changes to the atmospheric profile using radiosonde data (Fig. 3) and average surface weather conditions at the time of ignition are summarized in Table 3. Data from the European Centre for Medium-Range Weather Forecasts (ECMWF) Re-Analysis (ERA)-Interim are used to produce the synoptic analyses in this study (Dee *et al.* 2011). The ERA-Interim uses the ECMWF integrated forecasting system and a four-dimensional variational data assimilation system that ingests observations within a 12-h window around the analysis time.

1 November 2012: Burn Plots S3-S5

A high amplitude upper level trough affected the eastern United States on 1 November. Flow across the Florida panhandle was predominantly from the north and northwest providing weak cold air advection (Fig. 4*a*). The deep northerly flow is apparent in the morning (1641 UTC) and afternoon (2015 UTC) profiles (Fig. 3*a*). The morning profile indicates a shallow mixed layer extending from the surface to about 500 m, where an isothermal capping layer partially decouples the surface flow from the stronger flow aloft. By afternoon this capping layer has been removed and a deep adiabatic profile extends upwards to about1700 m ASL.

4 November 2012: Burn Plot L1G

On 4 November a low-amplitude upper-level trough was situated over the Ohio River valley with an associated region of weakly organized surface low pressure over South Carolina (Fig. 3*b*). Moderate west to northwest flow affected the region near the burn site during the day as a cold front approached from the northwest.

The morning sounding (Fig. 3*b*), taken at 1610 UTC (1010 LST), indicates a surface based mixed layer extending to a depth of ~600 m. The top of the mixed layer is delineated by a capping inversion across which temperature increases and dewpoint decreases sharply. Above the capping layer, an adiabatic residual layer, which is the remains of the previous day's mixed layer, extends upward to about 1000 m AGL. By late afternoon, the surface mixing eroded the capping inversion, coupling with the residual layer and substantially increased the mixing depth. Winds throughout the day were from the west to northwest.

7 November: Burn Plots S7-S9

During the third controlled burn a high-amplitude long wave trough dominated the weather over the eastern US (Fig. 3*c*). A mature surface cyclone presented east of Chesapeake Bay. Strong northwest flow behind an associated cold front affected the burn region. The front itself was located to the east of Florida at the time of the burn.

Consistent with the synoptic analysis, the soundings for 7 November reveal deep northwest flow in the post-cold-frontal air mass (Fig. 3*c*). The mean temperature is ~10°C colder than during the 4 November burn. Due to large scale destabilization of the airmass by cold-advection and enhanced mechanical mixing, the morning sounding reveals a deep mixed layer extending from the surface to about 1500 m. Later in the afternoon surface heating appreciably warmed the mixed layer and increased the mixing depth to ~1800 m.

10-11 November: Burn Plots L2G and L2F

For the final two burns, on 10 and 11 November, the weather was dominated by high pressure (Figs. 3*d* ,3*e*). On 10 November the axis of an upper level ridge was positioned over the eastern US with the center of surface high-pressure off the North Carolina coast. This configuration generated weak easterly flow across northern Florida. The following day, 11 November, the upper ridge and surface anti-cyclone shifted to the east as a trough slowly approached from the west. The wind across the Florida panhandle increased from the southeast, driving a warm moist onshore flow.

On 10 November the morning and afternoon soundings are dominated by the presence of a subsidence inversion associated with the upper level ridge (Fig. 3*d*). The inversion is apparent as a layer of warm and very dry air aloft. At 1600 UTC (10 LST), the base of this layer is situated at ~1100 m. The convective boundary layer subsequently erodes into this capping layer in the afternoon, providing a mixing depth of ~1300 m. The wind throughout the mixed layer is from the east and southeast at 5 to 10 kts.

On 11 November, as on the previous day, the subsidence inversion aloft is a key feature of both the morning and afternoon soundings (Fig. 3*e*). The morning sounding shows an additional stable layer at about 500 m, marking the remnants of the nocturnal decoupling. By afternoon convection has eroded through this intermediary capping layer and coupled with the residual layer aloft, allowing convective mixing up to ~1800 m. Winds throughout the period are strong from the southeast, consistent with the increased flow around the departing anti-cyclone.

Doppler lidar observations

The scanning Doppler lidar was used during each experimental burn to measure the spatial variability of the wind field and characteristics of the smoke plume dispersion. A plan position indicator (PPI) scan was used to collect radial velocities across a predetermined horizontal sector covering the burn plot. The PPI scans were conducted with an elevation angle of ~ 2°.

The lidar was placed on the upwind side of the perimeter of burn plots S5 and L2G in optimized locations that allowed the laser to be mostly uninterrupted by terrain, foliage, and other instrumentation. This strategy did have limitations however, in that at times the lidar beam was not able to penetrate through the densest part of the plume, thus restricting observations of flows on the downwind side of the plume. During the S5 burn, the lidar was situated on the northern perimeter of the burn unit. During the L2G burn, it was positioned on the eastern perimeter (Fig. 2). The range of the lidar was nearly 1000 m for most experiments with a gate length of 18 m.

S5 Burn Plot

During the S5 burn, the lidar was set up to perform PPI sector scans between 163° and 215° azimuths at an elevation of 2°. A north wind was dominant for the duration of the experiment. The small contour shown at 17:23:57 UTC in Fig. 5*a* indicates where the lidar beam hit instrument towers within the burn plot. Just after ignition, the lidar measured smoke plume development at 17:23:57 UTC (Fig. 5*b*) where higher values of backscatter intensity indicate the plume's boundaries indicated by the solid contours in Fig. 5. At 17:28:00 UTC (Fig. 5*c*), the smoke was observed propagating towards the southwest, transported by northeasterly surface winds. The upwind side of the plume boundary indicates the region of the fire front. A shift in the wind direction from northeasterly to northwesterly occurred at 17:29:59 UTC (Fig. 5*d*). The velocity of the northwesterly surface wind was slightly higher than the northeasterly winds. During the northeasterly flow, the width of the smoke column was 150 m indicating that the plume remained close to the surface. At times, the lidar beam becomes attenuated downwind of the smoke column, reducing the signal-to-noise ratio, as indicated by the highly variable radial velocities (Fig. 5*d*; y=-500 m, x= 0 m). However, there are regions within the plume where radial velocities increase in magnitude, indicating fire-induced winds associated with fire-atmosphere interactions. This is quite surprising given the low intensity of these fires. At 17:28:00 UTC the plume structure is pointed at the most downwind location (x = -190 m, y= -350 m). This structure does resemble the shape of the head fire. A maxima in radial velocity of ~7 m s^{-1} occurs in this region, associated with fire-induced flow near the fire front. The PPI scans provide measurements of the spatial variability in the surface wind speed ranging from 2 to 7 m s^{-1} across the plot.

L2G Burn Plot

During L2G, the lidar was positioned on the southeast corner of the plot and performed PPI scans between 240° and 320° azimuths at an elevation of 2°. To characterize the wind profile at the time of ignition, the lidar also made three vertical wind profile measurements during the 10 minutes before ignition, and these were averaged to provide a single profile (Fig. 6). The wind speed ranged between 3 and 5 m s^{-1} above 200 m AGL up to 1200 m AGL. Weak wind shear was also present between the lowest measurement level at 60 m, up to 200 m AGL. Wind direction was fairly constant, remaining southeasterly throughout the profile.

Most notable in the PPI scans shown in Fig. 7 are the regions of higher radial velocities scattered throughout the scan. These regions represent wind gusts of 3 to 6 m s^{-1}, while ambient background winds (radial velocities) are between 0 and 2 m s^{-1}. This flow structure is shown at 18:24:15 UTC (Fig. 7*a*) before the ignition occurred. At 18:27:06 UTC (Fig. 7*b*) ignition had just begun with two strip head fires, shown by the two parallel regions of higher backscatter intensity, indicating the plume boundaries of two fire lines. Radial velocities within and near the plume boundaries increasef, suggesting that the fire front caused acceleration of ambient winds into the fire and plume base. As the ignition continued (Fig. 7*c*), the plume boundaries merge as smoke from each fire line mixes downwind. At this time, the radial velocities increased both within the plume and downwind of the plume. There were, however, regions downwind of the plume where the velocity decreased to nearly calm. This is indicated by regions of 0 m s^{-1} (-500 m, 390 m) (Fig. 7*c*). These flow structures could potentially be intermittent zones of convergence, where flows decrease in velocity in response to the warmer air in the plume. Similar structures have been observed in grass fires on sloped terrain (Charland and Clements 2013). Another interesting feature is the larger zone of weaker winds that develop a few minutes later at 18:31:06 UTC (Fig. 7*d*). At the downwind side of the plume (150 m, -850 m, and dashed line), winds reversed in direction, indicating a circulation that developed in response to the fire and plume. The dashed line in Fig. 7*d* indicates the boundary between the outbound and inbound winds, which increased to nearly 2.5 m s^{-1}. The boundary of the convergence zone is no longer present in the next scans at 18:33:02 UTC (Fig. 6*e*) and 18:35:06 UTC (Fig. 6*f*), suggesting that the circulation was short lived and may have been a result of intermittent flow blocking caused by the plume. Further observations are needed to substantiate this hypothesis.

Micrometeorology during fire front passage (FFP)

S5 Burn Block

The microscale wind structure and turbulent heat fluxes of the fire front were measured using the two sonic anemometers mounted on the in situ tower. Streamwise, crosswise, and vertical velocities, and sonic temperature, were measured at 2.0 and 5.8 m AGL (Fig 8*a*-*d*). As the FFP occurred, the streamwise wind velocity, u, decreased to zero and then became negative between 18:15:30 and 18:16:00 UTC (Fig. 8*a*) and was most likely caused by fire-induced circulations generated by increased thermal instability of the near-surface air at the fire front. The crosswise wind velocity, v, in Fig. 8*b* showed little influence of the fire front passage (FFP). Increases in both the upward vertical velocity, w, (Fig. 8*c*) and T_s (Fig. 8*d*) at 5.8 m AGL indicate that a forward-tilted smoke column reached the upper part of the tower between 18:13:00 and18:14:30 UTC with peak T_s ~ 74 °C, while the 2.8-m level shows smaller fluctuations in vertical velocity and T_s (Fig. 8*d*). The fluctuations became larger at the 2.0 m AGL than 5.8 m AGL after 18:14:45 UTC as the fire front approached the tower. A peak sonic temperature of 224°C at 2.0 m AGL was measured at 18:15:43 UTC. Strong downdrafts have been observed in previous studies around the time of fire front passage (Clements *et al.* 2007). However, no significant downdrafts were observed during FFP, due perhaps to the fact that the fire was of lower intensity, limiting fire-atmosphere coupling.

Figure 9*a* shows radiative heat flux measured at 2.7 m AGL using a Schmidt Boelter radiometer. A peak value of 4.9 kW m^{-2} was measured during FFP, and the increased radiative heat flux corresponds to the increase in T_s at 2.8 m AGL (Fig. 8*d*). The peak value is similar to observations by Silvani and Morandini (2009), further suggesting the S5 fire was representative of low-intensity fires. The 1-min averaged turbulence kinetic energy (TKE) remained relatively constant at both levels during the FFP even though radiative heat flux increased (Fig. 9). The maximum 1-min averaged sensible heat flux, H_s, at 5.8 m AGL was 12.7 kW m^{-2}, when the plume reached the upper part of the tower, whereas the maximum H_s measured at 2.8 m AGL was 9.3 kW m^{-2}.

L2G Burn Block

Similar turbulent flux measurements were made during the L2G burn. Both *u* and *v* velocities in Fig. 10 show noticeable, but rather weak, perturbations at 1.9 m AGL between 18:51:40 and 18:52:00 UTC due to FFP. Similar to S5 burn, the FFP had very limited influence on horizontal wind field although the *v* velocity varied more during the L2G burn than during the S5 burn. Observed increase in vertical velocity at 5.8 m AGL between 18:50:00 and 18:51:20 UTC indicate plume updraft located ahead of the fire front, whereas the increased updraft velocity measured at 1.9 m AGL occurred when the fire front was at the base of the tower. A maximum T_s of 237°C measured at 1.9 m AGL was slightly higher than that measured at S5 site. However, the sonic temperatures reached around 200°C more consistently during the L2G burn than during the S5 burn, indicating larger heat release from the fire into the atmosphere. The sonic temperature measured at 5.8 m AGL remained below 100 °C, possibly due to entrainment of ambient air into the base of the convective column.

The total heat flux, which accounts for both convective and radiative components of heat flux, increased between 18:50:00 and 18:51:40 UTC (Fig. 11), while the sensible heat flux did not. This is because of the downwind-tilted convective plume from the fire initially dominated the near-surface environment ahead of the FFP. As the fire front approached the tower, the radiative heat flux began to increase. The radiative heat flux reached 18 kW m^{-2}, which is more than three times larger in magnitude than that measured during the S5 burn.

The measured TKE associated with FFP was larger than measured values from the S5 burn, with maximum values of 3.6 $m^2 s^{-2}$ and 3.1 $m^2 s^{-2}$ at 5.8 m and 1.9 m AGL, respectively. Turbulence kinetic energy during the FireFlux experiment (Clements *et al.* 2008) was ~10 $m^2 s^{-2}$, so the TKE generated during the L2G burn represent low turbulence intensity associated with FFP. The total heat flux instantaneously reached a peak value of 26 kW m^{-2}. The sensible heat flux measurements indicate that larger heat release from the fire occurred during the L2G burn than S5 burn. An observed maximum sensible heat flux value during L2G was 37.5 kW m^{-2} measured at 1.9 m AGL, which was about four times greater than the value observed at S5. Furthermore, the H_s at 5.8 m AGL was about half of the H_s observed at 1.9 m AGL, which may be caused by entrainment of cooler ambient air into the plume.

Summary and conclusions

The RxCADRE campaign represents a major effort in the simultaneous monitoring of fire weather and micrometeorology, with fine-scale fuels and fire behavior sampling during multiple low-intensity prescribed fire experiments. The experimental design was aimed at exploiting a high-spatial resolution network of instrumentation to measure the small-scale meteorology within and around each burn block. Fire weather conditions were favorable for conducting each experiment with favorable ambient wind speed and direction, temperature and humidity, and dispersion characteristics.

The experimental array consisted of a suite of cup-and-vane anemometers that lined each burn block perimeter, an in situ micrometeorological tower that measured fire-induced circulations, sensible heat flux, and turbulence statistics associated with the fire front. Additionally, vertical wind profiles were obtained by a Doppler SoDAR placed upwind of each burn block and by a scanning Doppler lidar, which also measured horizontal winds spatially across each burn block and provided measurements of plume height. Upper-air radiosonde soundings were made for each burn just before ignition and after burning was complete. The CSU-MAPS mobile 32-m meteorological tower was deployed during each experiment to measure profiles of wind speed and direction, temperature and relative humidity, and turbulence statistics.

Preliminary results show that the meteorological measurement campaign during RxCADRE was successful in capturing both the fire weather conditions that influenced the experiments and the local fire-atmosphere interactions at the fire front. The Doppler lidar provided a high-resolution and large areal coverage of radial velocities across each burn block. Fire-induced circulations were observed to occur during the L2G burn where strip head fires created a merged plume. A region of decreased radial velocities and reversed flow was observed to occur downwind of the plume and was most likely associated with the development of a convergence zone forming in response to instabilities associated with the fire front. The convergence zone was not observed during the S5 burn block most likely due to the smaller size of the fire line and overall lower-intensity of the fire.

The turbulence sensible heat fluxes measured during the fire front passage varied between 5 and 35 kw m^{-2} and compare well with measurements made by the passive heat flux radiometers, ~ 18 - 20 kW m^{-2}. The turbulent kinetic energy ranged from ~1 $m^2\,s^{-2}$ for ambient conditions and up to 5 $m^2\,s^{-2}$ during the fire. These measured values indicate that the S5 and L2G fires were very lower intensity as compared to other grass fires and or forest fires.

Acknowledgements

The authors would like to acknowledge many individuals from Eglin Air Force Base Jackson Guard that helped us meet our specific research goals including Mr. Keith Hawk, Mr. David Grimm, and Brett Williams who was the overall incident commander for the experiments. In addition, we would like to acknowledge Wyndam Lewis for his help in the field. The meteorological measurement campaign was supported by funding from the Joint Fire Science Program (Project #11-2-1-11) and the National Science Foundation (AGS-1151930).

References

Dee DP, Uppala SM, Simmons AJ, Berrisford P, Poli P, Kobayashi S, Andrae U, Balmaseda MA, Balsamo G, Bauer P, Bechtold P, Beljaars ACM, van de Berg L, Bidlot J, N. Bormann, Delsol C, Dragani R, Fuentes M, Geer AJ, Haimberger L, Healy SB, Hersbach H, Hólm EV, Isaksen L, Kållberg P, Köhler M, Matricardi M, McNally AP, Monge-Sanz BM, Morcrette JJ, Park BK, Peubey C, de Rosnay P, Tavolato C, Thépaut JN, Vitart F (2011)The ERA-Interim reanalysis: configuration and performance of the data assimilation system. *Quarterly Journal of the Royal Meteorological Society* **137**, 553–597. doi: 10.1002/qj.828

Charland A, Clements CB (2013) Kinematic structure of a wildland fire plume observed by Doppler lidar. *Journal of Geophysical Research-Atmospheres* **118**, 3200–3212. doi:10.1002/jgrd.50308

Clements CB, Oliphant AO (2014) The California State University- Mobile Atmospheric Profiling System (CSU-MAPS): A facility for research and education in boundary-layer meteorology. *Bulletin of the American Meteorological Society*. In Press. doi:10.1175/BAMS-D-00179.1

Clements CB (2010) Thermodynamic structure of a grass fire plume. *International Journal of Wildland Fire* **19**, 895–902. doi: 10.1071/WF09009

Clements CB, Zhong WS, Bian X, Heilman WE, Byun DW (2008) First observations of turbulence generated by grass fires. *Journal of Geophysical Research* **113,** D22102. doi:10.1029/2008JD010014

Clements, CB, Zhong S, Goodrick S, Li J, Bian X, Potter BE, Heilman WE, Charney JJ, Perna R, Jang M, Lee D, Patel M, Street S, Aumann G (2007) Observing the dynamics of wildland grass fires: FireFlux—field validation experiment. Bulletin of the American Meteorological Society **88**, 1369–1382. doi:10.1175/BAMS-88-9-1369

Coen JL, Cameron M, Michalakes J, Patton EG, Riggan PJ, Yedinak KM (2013) WRF-Fire: coupled weather-wildland fire modeling with the weather research and forecasting model. Journal of Applied Meteorology **52**, 16–38. doi: 10.1175/JAMC-D-12-023.1

Horel JD, Dong X (2010) An evaluation of the distribution of remote automated weather stations (RAWS). Journal of Applied Meteorology and Climatology **49**, 1563–1578. doi: 10.1175/2010JAMC2397.1

Filippi J-B, Pialat X, Clements CB (2013) Assessment of ForeFire/Meso-NH for wildland fire/atmosphere coupled simulation of the FireFlux experiment. *Proceedings of the Combustion Institute* **34**, 2633–2640. doi: 10.1016/j.proci/2012.07.022

Kochanski A, Jenkins M, Mandel J, Beezley J, Clements CB, Krueger S (2013) Evaluation of WRF-Sfire performance with field observations from the FireFlux experiment. *Geoscientific Model Development* **6**, 1109–1126. doi:10.5194/gmd-6-1109-2013

Pearson G, Davies F, Collier C (2009) An analysis of the performance of the UFAM pulsed Doppler lidar for observing the boundary layer, *Journal of Atmospheric And Oceanic*

Technology **26**, 240–250. doi:10.1175/2008JTECHA1128.1

Pearson G, Davies F, Collier C (2010) Remote sensing of the tropical rain forest boundary layer using pulsed Doppler lidar. *Atmospheric Chemistry and Physics* **10,** 5891–5901. doi:10.5194/acp-10-5891-2010

Potter BE (2012) Atmospheric interactions with wildland fire behaviour. Basic surface interactions, vertical profiles and synoptic structures. *International Journal of Wildland Fire* **21**, 779–801. doi:10.1071/WF11128

Silvani X, Morandini F (2009) Fire spread experiments in the field: temperature and heat fluxes measurements. *Fire Safety Journal* **44**, 279. doi: 10.1016/j.firesaf.2008.06.004

Ware R, Carpenter R, Güldner J, Liljegren J, Nehrkorn T, Solheim F, Vandenberghe F (2003) A multichannel radiometric profiler of temperature, humidity, and cloud liquid. *Radio Science* **38**, 8079. doi:10.1029/2002RS00285

Table 1. Meteorological instrumentation used in RxCADRE

Platform	Sensor type and model	Variables	Measurement height (m AGL)	Sampling frequency
Micrometeorology tower	3-D sonic anemometer (Applied Technologies Inc. SATI Sx)	u, v, w, t_S	2.0 and 5.8 (3.8 and 8.7 for L2F)	10 Hz
	Type-E thermocouples (Omega Inc. 5SC-TT-E)	T	1.0–6 m	5 Hz
	Total heat flux (Hukseflux SBG01)	Q (kW m^{-2})	2.8	5 Hz
	Radiative heat flux (Medtherm 64 series)	Q (kW m^{-2})	2.7 (8.3 for L2F)	5 Hz
CSU-MAPS 32-m extendable tower	Thermistor/hygristor sensors (Vaisala, Inc. HMP45C)	T, RH	7.0–31.0	1 min
	3-D sonic anemometers (RM Young 81000)	u, v, w, t_S	7.0 & 31.0	10 Hz
Doppler mini SoDAR	(Atmospheric Research &	u, v, w	15.0–200	1 Hz

	Technology VT-1)			
CSU-MAPS mobile profilers	Doppler lidar (Halo Photonics, Ltd., Streamline 75)	*v_r**, *β**	range gate: 18 m	1 Hz
	Microwave profiler (Radiometrics Corp., MP-3000A)	*T*, *RH*	50 m–10 km	180 s
Cup and vane anemometers	Wind speed and direction (Onset Computer Corporation, S-CA-M003)	*WS/WD*	3.3	3 s

**v_r* = radial velocity, *β*=aerosol backscatter intensity

Table 2. Burn plot instrumentation and ignition information

Burn unit	Number of anemometers	Burn date (2012)	Burn start time (UTC)	Data collection end time (UTC)
S3	32 adjacent to plot; 2 NW of plot	1 November	21:20	22:30
S4	40 adjacent to plot; 3 NW of plot	1 November	19:35	21:15
S5	32 adjacent to plot; 3 NW of plot	1 November	18:10	19:30
S6	10 adjacent to plot (TEST PLOT)	31 October	19:11	20:00
S7	33 adjacent to plot; 3 NW of plot	7 November	17:25	18:50
S8	25 adjacent to plot	7 November	20:16	21:30
S9	23 adjacent to plot	7 November	18:54	20:10
L1G	76 adjacent to plot	7 November	18:31	23:59
L2F	34 adjacent to plot; 1 @ each HIP; 12 crossing interior firebreak	11 November	18:02	23:59
L2G	35 adjacent to plot; 1 @ each HIP;12 crossing interior firebreak	10 November	18:23	23:59

Table 3. Average meteorological surface conditions at ignition

Burn unit	Temperature (°C)	Relative humidity (%)	Wind speed (m s^{-1})	Wind direction (°)
S3, S4, S5	22.0	28.0	4.0	345
S7, S8, S9	17.0	50.0	3.5	300
L2F	24.0	60.0	3.0	130
L2G	23.0	41.0	2.0	130

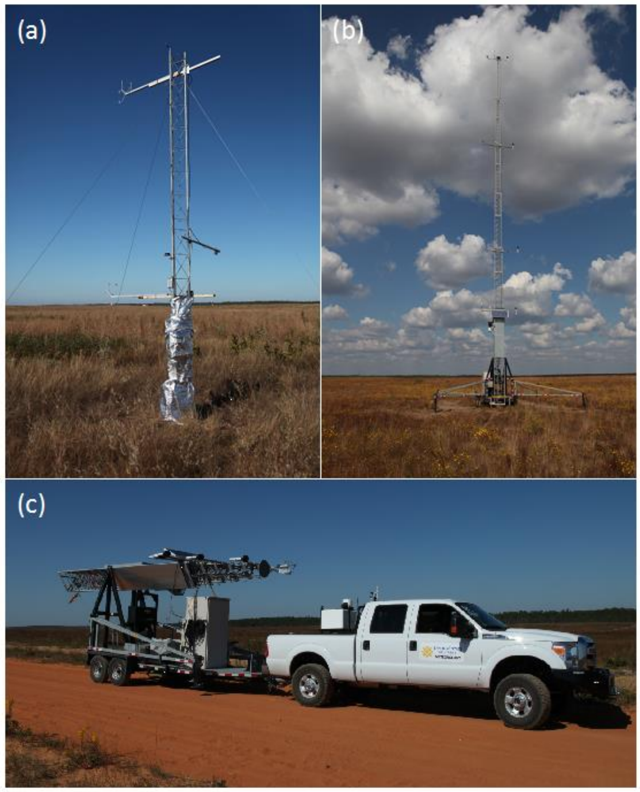

1 **Fig. 1.** Photographs of (*a*) 6-m micrometeorological tower, (*b*) CSU-MAPS tower deployed within L1G burn unit, and (*c*) complete CSU-MAPS system.

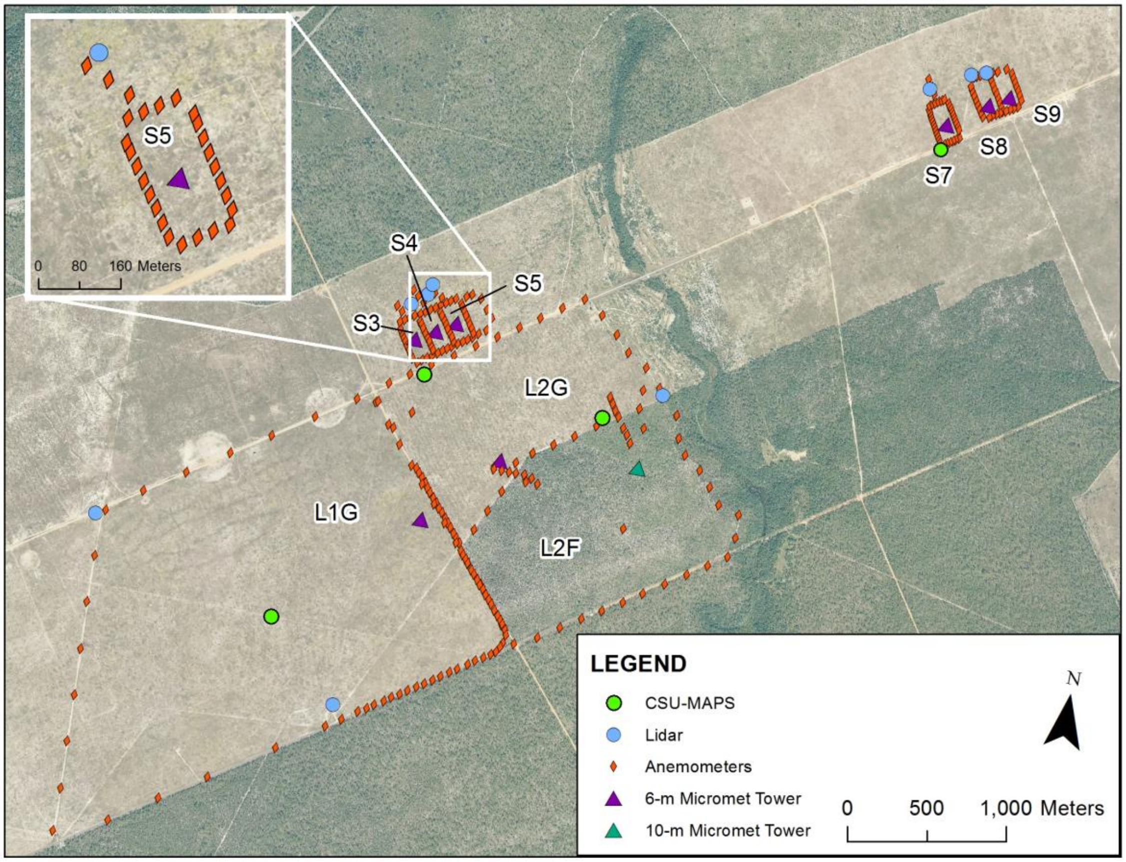

Fig. 2. Map showing details of burn plots and main meteorological instrument locations.

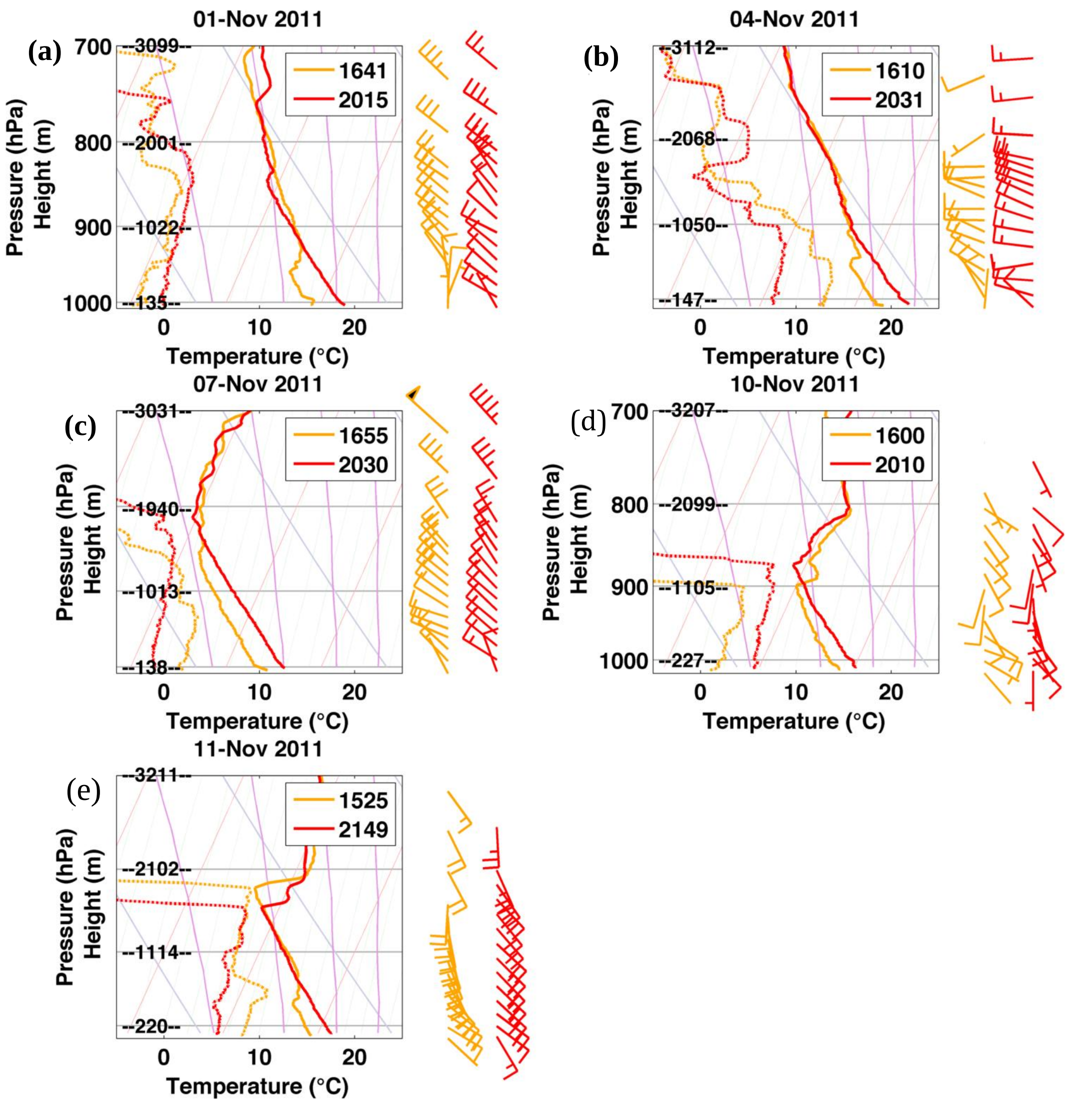

Fig. 3. Skew-T log-P diagrams for the prefire (orange) and postfire (red) radiosondes for each burn day (*a* through *e*). Each panel shows the air temperature (solid lines), dew point temperature (dashed lines), and the wind profile (barbs). Listed times are UTC.

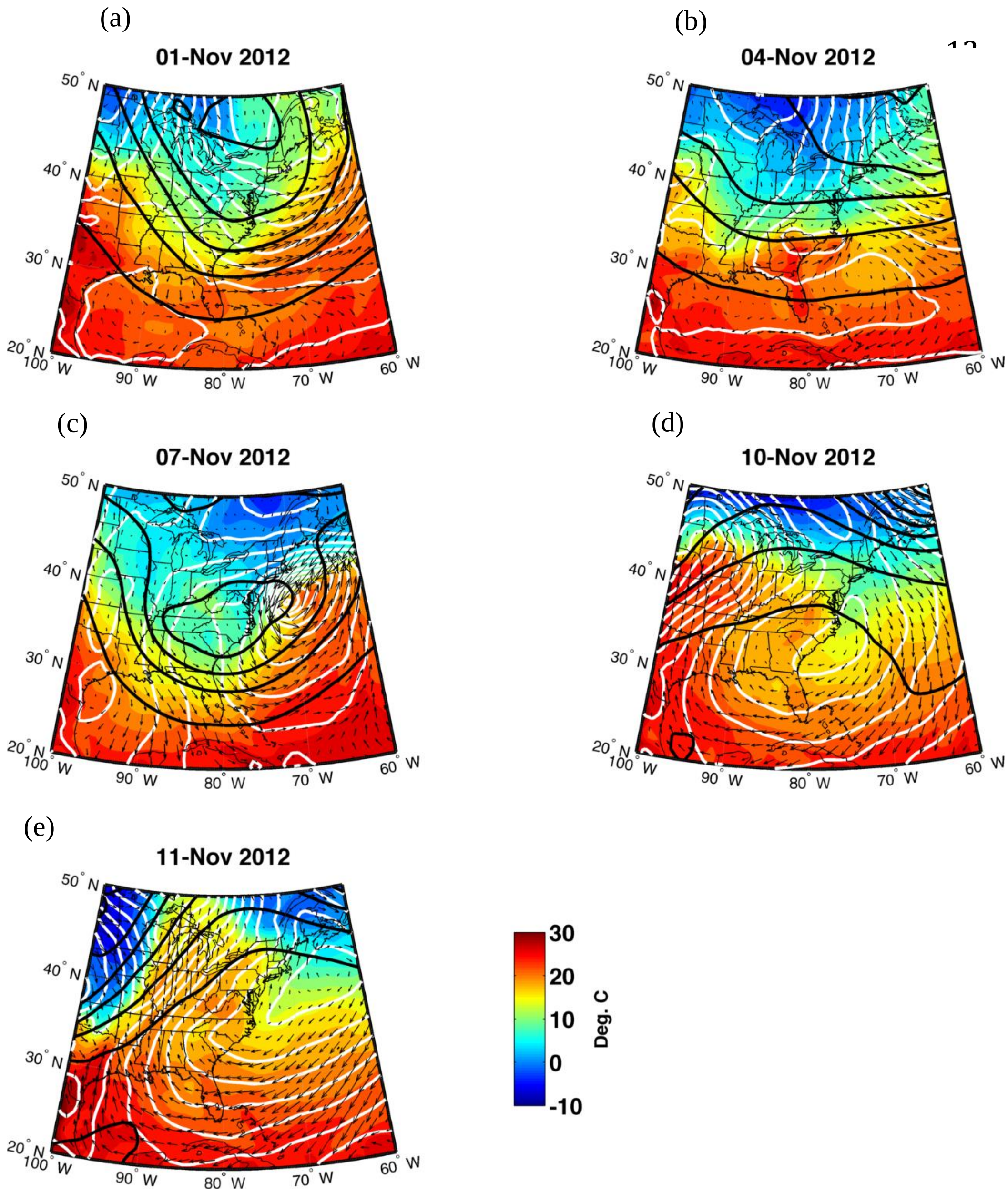

Fig. 4. Synoptic-scale weather conditions during each controlled burn. Each panel shows the 500-hPa geopotential height (black contours, 100-m contour interval), the 1000-hPa geopotential height (white contours, 25-m coutour interval), the 2-m air temperature (color shading), and the 10-m wind vectors. Plots burned on each day are: (*a*) S3, S4, and S5, (*b*) L1G, (*c*) S7, S8, and S9, (*d*) L2G, and (*e*) L2F.

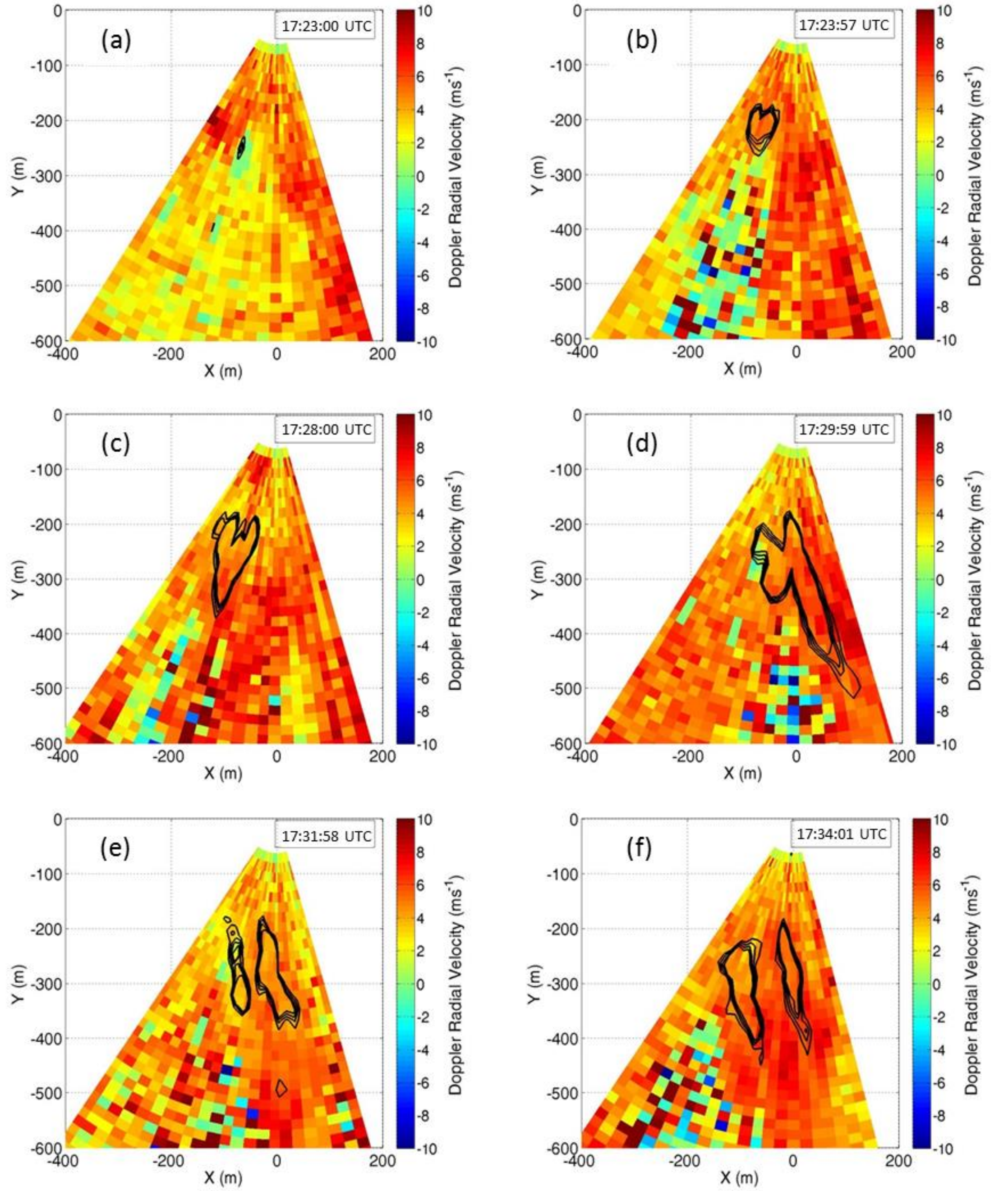

Fig. 5. Burn plot S5 lidar plan position indicator (PPI) scans through time. Radial velocities are displayed in color. The black contours of backscatter intensity represent the boundaries of the smoke column.

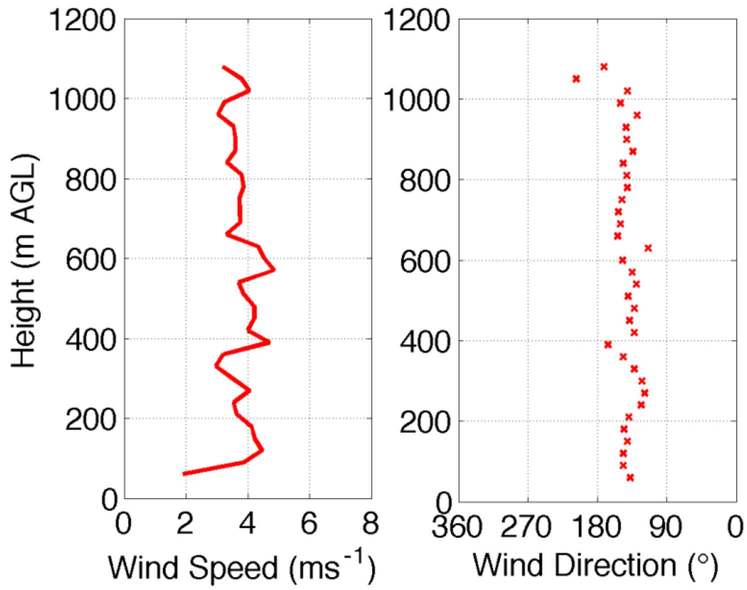

Fig. 6. Ten-minute mean wind profile measured from the lidar before ignition at the L2G burn plot.

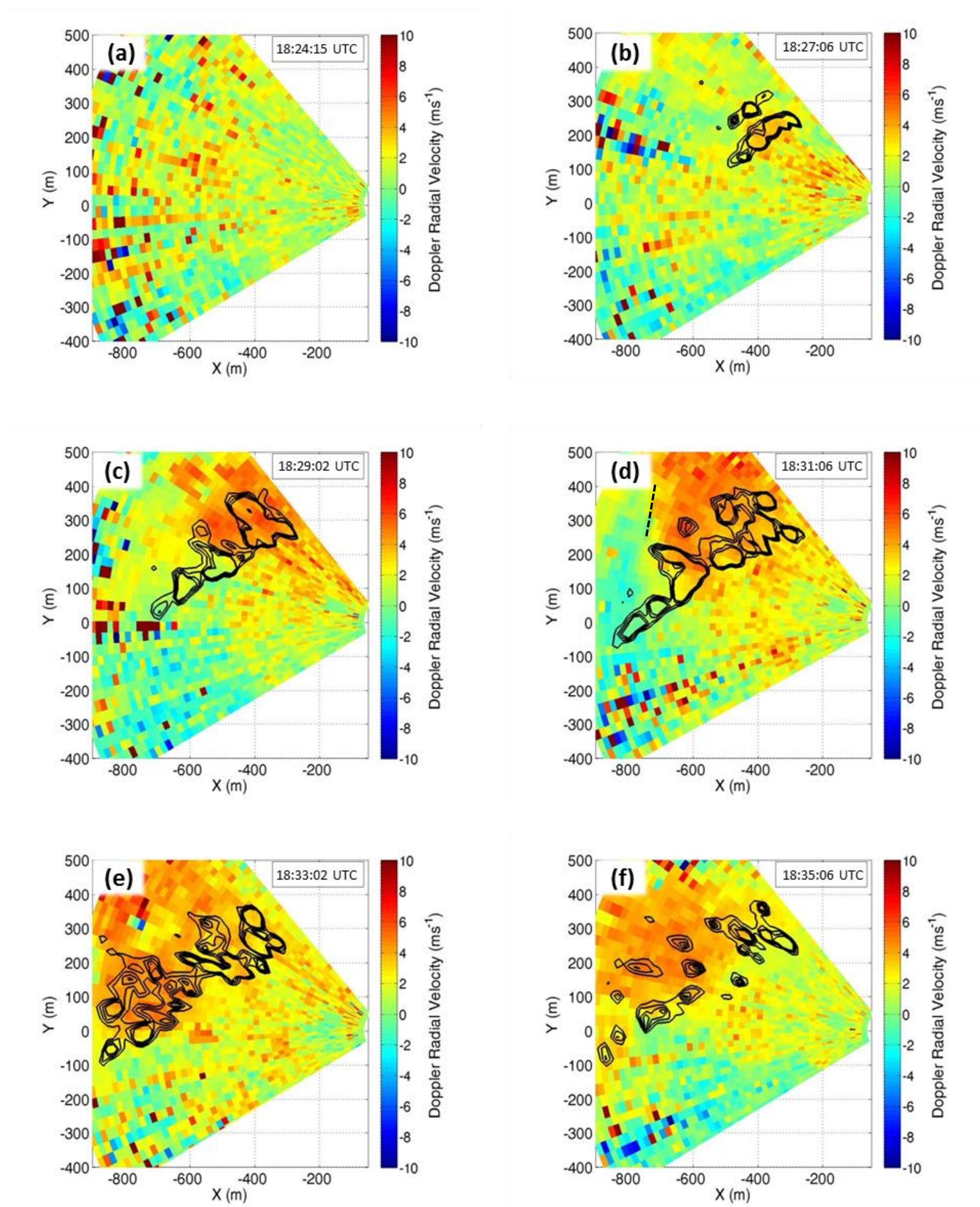

Fig. 7. Burn plot L2G lidar plan position indicator (PPI) scans through time. Radial velocities are displayed in color. The black contours of backscatter intensity represent the smoke plume boundaries. Dashed line in panel (*d*) indicates convergence zone.

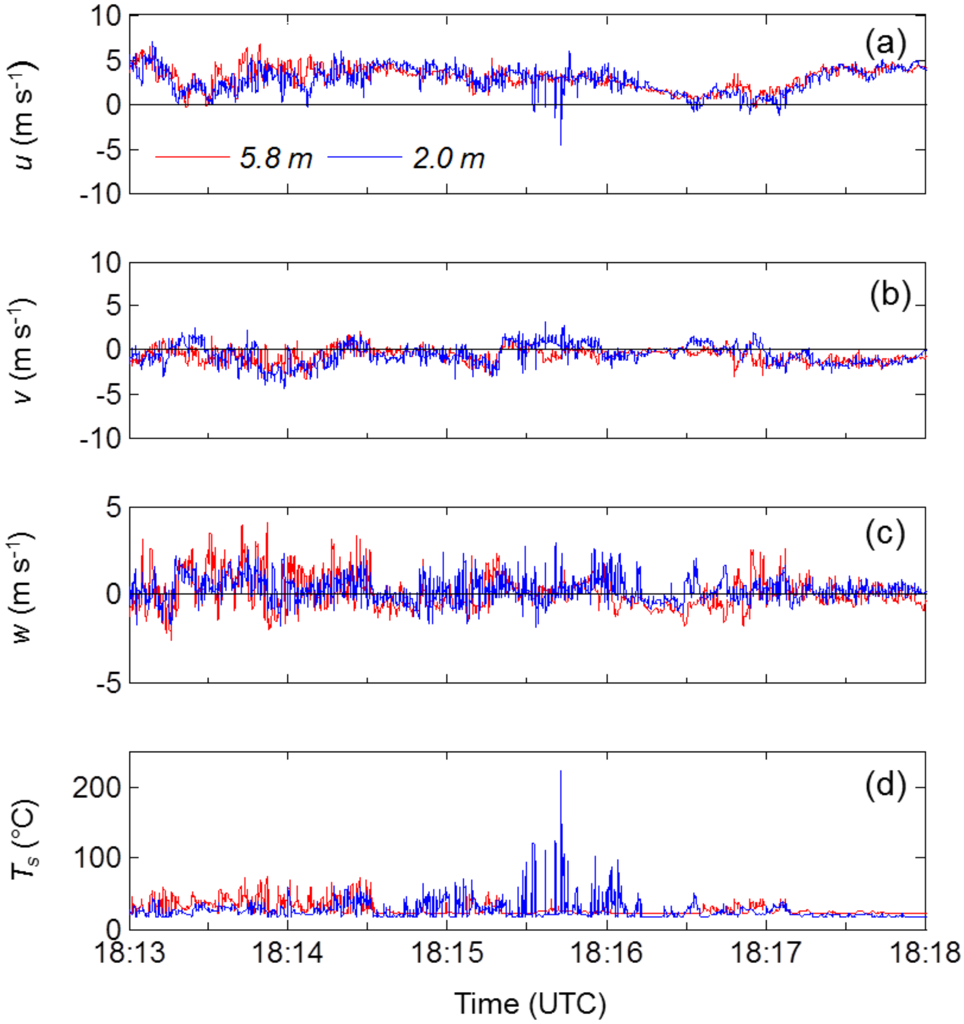

Fig. 8. Time series of 10-Hz (a) streamwise (b) crosswise and (c) vertical wind velocities and (d) sonic temperatures measured during S5 burn on 1 November 2012.

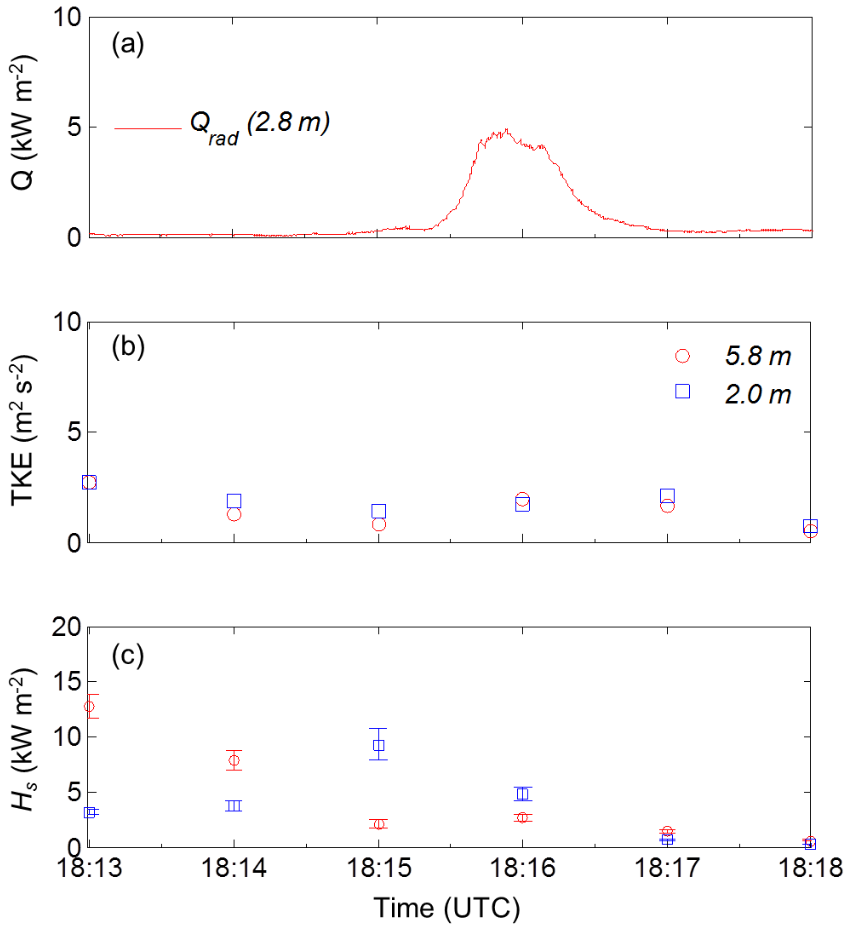

Fig. 9. Time series of (a) 10-Hz radiative heat flux, (b) 1-min averaged turbulence kinetic energy (TKE), and (c) sensible heat flux, measured during S5 burn on 1 November 2012.

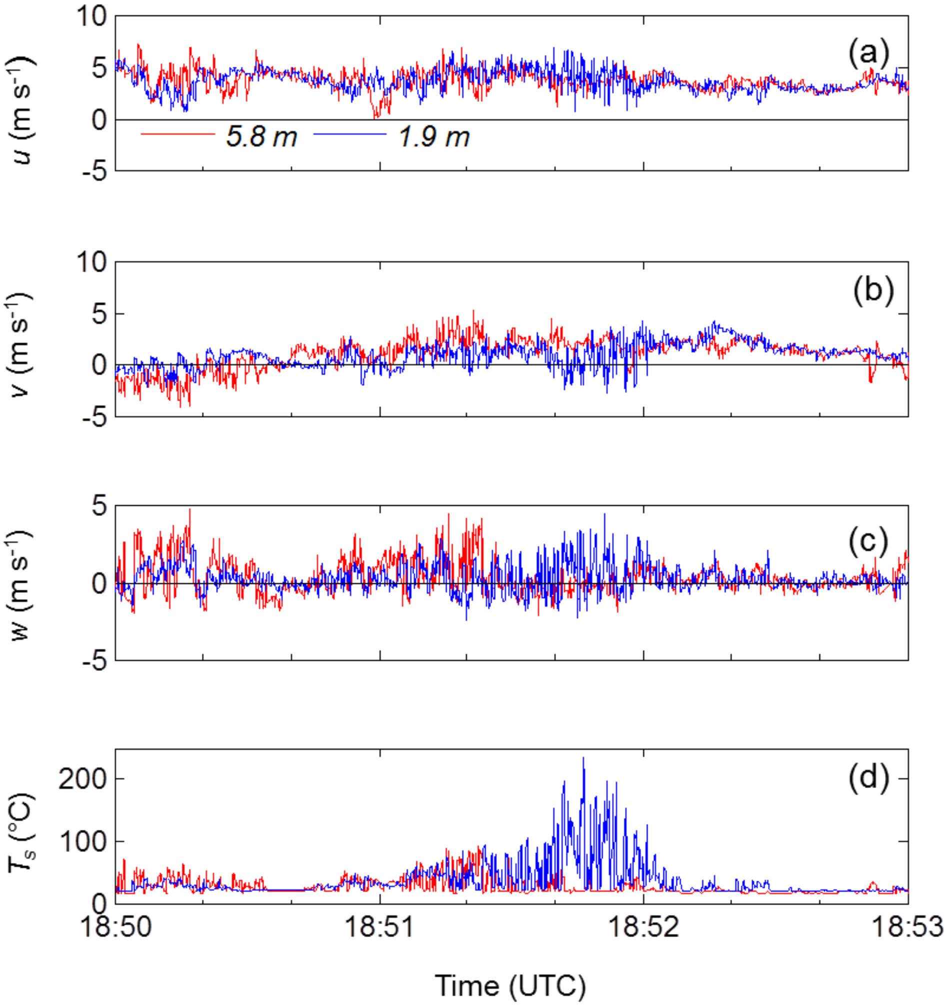

Fig. 10. Time series of 10-Hz wind velocities (a) streamwise, (b) crosswise, and (c) vertically, and of (d) sonic temperatures measured during L2G burn on 10 November 2012.

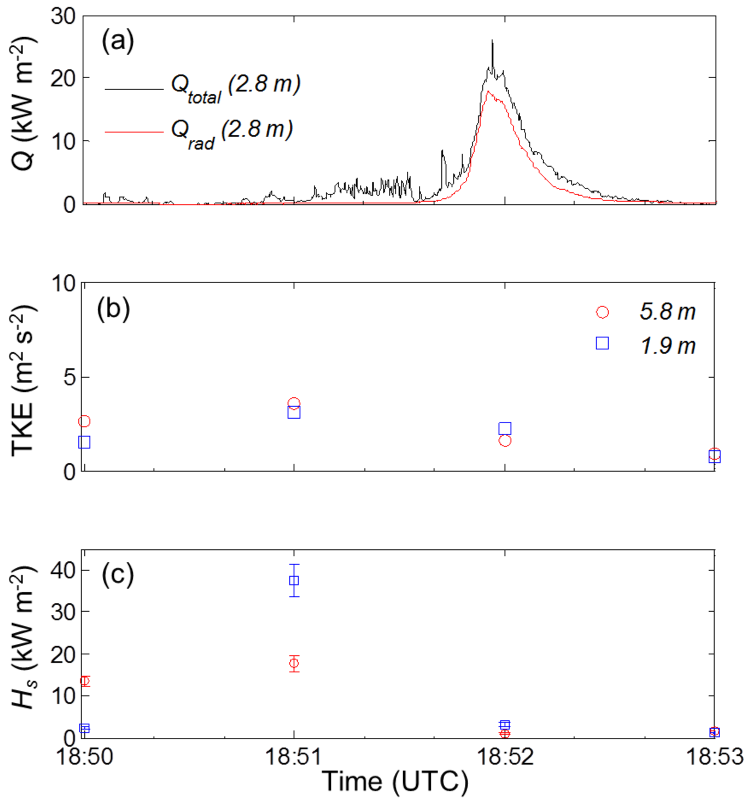

Fig. 11. Time series of (a) 10-Hz total and sensible heat fluxes, (b) 1-min averaged turbulence kinetic energy (TKE) and (c) sensible heat flux, measured during S5 burn on 10 November 2012.